
A FRAMEWORK FOR ANALYZING ONLINE CROSS-CORRELATORS USING PRICE'S THEOREM AND PIECEWISE-LINEAR DECOMPOSITION

Zhili Xiao

Electrical & Systems Engineering
Washington University in Saint Louis
Saint Louis, MO 63130
xiaozhili@wustl.edu

Shantanu Chakrabartty

Electrical & Systems Engineering
Washington University in Saint Louis
Saint Louis, MO 63130
shantanu@wustl.edu

ABSTRACT

Precise estimation of cross-correlation or similarity between two random variables lies at the heart of signal detection, hyperdimensional computing, associative memories, and neural networks. Although a vast literature exists on different methods for estimating cross-correlations, the question *what is the best and simplest method to estimate cross-correlations using finite samples?* is still not clear. In this paper, we first argue that the standard empirical approach might not be the optimal method even though the estimator exhibits uniform convergence to the true cross-correlation. Instead, we show that there exists a large class of simple non-linear functions that can be used to construct cross-correlators with a higher signal-to-noise ratio (SNR). To demonstrate this, we first present a general mathematical framework using Price's Theorem that allows us to analyze cross-correlators constructed using a mixture of piece-wise linear functions. Using this framework and high-dimensional embedding, we show that some of the most promising cross-correlators are based on Huber's loss functions, margin-propagation (MP) functions, and the log-sum-exp functions.

1 Introduction

Estimating cross-correlations between random variables plays an important role in the field of statistics [1], machine learning [2, 3], and signal detection [4, 5]. This is because the cross-correlation metric measures some form of similarity between the random variables, and hence reveals how one might influence the another. With proper normalization, the metric becomes equivalent to cosine similarity and unitary transforms, both of which are extensively used in linear algebra [6], natural language processing [7], and computer vision [8, 9]. In the emerging field of Hyperdimensional Computing [10, 11] cross-correlations are generally associated with inner products used for information retrieval from sparse distributed memories.

In its most general form cross-correlation $R : \mathcal{R} \times \mathcal{R} \rightarrow \mathcal{R}$ is defined for a pair of zero-mean, unit-variance random variables $x \in \mathcal{R}$, $y \in \mathcal{R}$ as

$$R := \mathcal{E}[xy] = \int_{-\infty}^{\infty} \int_{-\infty}^{\infty} xy p(x, y) dx dy. \quad (1)$$

where $p : \mathcal{R} \times \mathcal{R} \rightarrow \mathcal{R}^+$ denotes the underlying joint probability distribution from which x and y are drawn from. The operator $\mathcal{E}[\cdot]$ denotes an expectation under the probability measure p . In practice the distribution p is not known apriori, instead, one has access to N samples independently drawn from the distribution p . If we denote the sample vectors as $\mathbf{x} \in \mathcal{R}^N$ and $\mathbf{y} \in \mathcal{R}^N$, then the empirical cross-correlation can be estimated as

$$\hat{R}_N = \frac{1}{N} \sum_{n=1}^N x_n y_n \quad (2)$$

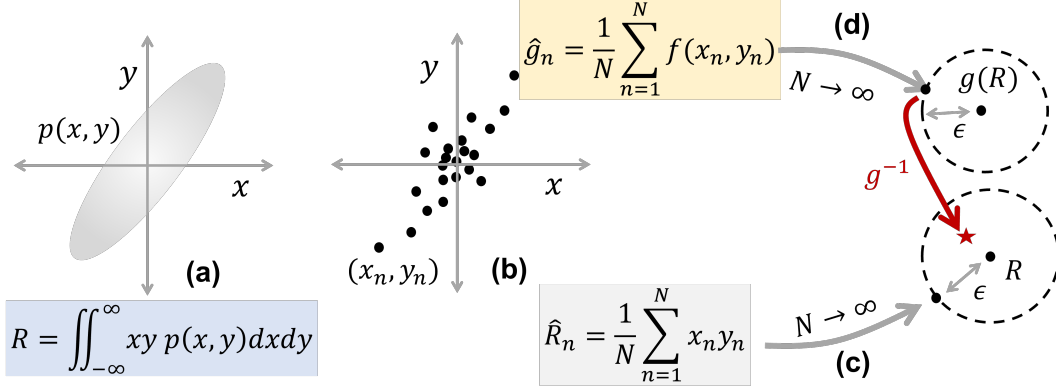


Figure 1: (a) Statistical definition of cross-correlation R between random variables x and y under a joint distribution $p(x, y)$; (b) Empirical cross-correlation \hat{R}_N based on samples (x_n, y_n) ; (c) Uniform convergence of \hat{R}_N to R ; (d) Uniform convergence of empirical non-linear cross-correlator \hat{g}_N to $g(R)$; and (e) Estimation of R using g^{-1} .

where x_n, y_n represent the elements of the vector \mathbf{x} and \mathbf{y} . Then, by the law of large numbers (LLN), the empirical correlation converges uniformly to the true correlation R

$$\left| \frac{1}{N} \sum_{n=1}^N x_n y_n - R \right| \leq \epsilon \xrightarrow{N \rightarrow \infty} 0 \quad (3)$$

and is depicted in Fig. 1. Note that equation 2 admits an online approach for estimating \hat{R}_N according to

$$\hat{R}_N = \left(1 - \frac{1}{N}\right) \hat{R}_{N-1} + \frac{1}{N} x_N y_N \quad (4)$$

In this paper, we explore an alternate approach towards estimating cross-correlations using a class of non-linear functions $f: \mathcal{R} \times \mathcal{R} \rightarrow \mathcal{R}$ such that

$$\frac{1}{N} \sum_{n=1}^N f(x_n, y_n) \xrightarrow{N \rightarrow \infty} \mathcal{E}[f(x, y)] = g(R) \quad (5)$$

where $g: \mathcal{R} \rightarrow \mathcal{R}$ is a monotonic function. The uniform convergence of f is illustrated in Figure. 1 where

$$\left| \frac{1}{N} \sum_{n=1}^N f(x_n, y_n) - g(R) \right| \leq \epsilon \xrightarrow{N \rightarrow \infty} 0 \quad (6)$$

The main premise of this paper is that when x and y are drawn from a joint Gaussian distribution, the function g is known a priori or can be estimated with high accuracy. As a result, and as illustrated in Figure 1, for a finite sample size N , an estimate of the correlation using $g^{-1}\left(\frac{1}{N} \sum_{n=1}^N f(x_n, y_n)\right)$ could be closer than \hat{R} to the true cross-correlation R . Under what conditions this might be true will be the main topic of investigation for this paper. Note that the focus of this paper

The paper is organized as follows: In section 2, we first propose a mathematical framework that can be used to analyze cross-correlators for a general class of non-linear function f , and for jointly distributed Gaussian inputs. We use the framework to analyze different types of estimators which include the linear-rectifier cross-correlator, Margin Propagation (MP) correlators, Huber-type cross-correlators, and log-sum-exp (LSE) estimators. In section 3, we extend the framework to arbitrary input distributions based on Hyperdimensional mapping using Walsh-Hadamard transforms. In section 4, we show experiments evaluating different correlators and the transformation method, and discuss the advantages and disadvantages of their possible hardware implementations. Section 5 concludes the paper with a brief perspective on future directions.

2 Analysis Framework using Price's Theorem

In this section we present an analysis framework that can be used to understand the behavior of different cross-correlators. A cross-correlator can be viewed as a difference between two functions and in Fig. 2(a) we illustrate this

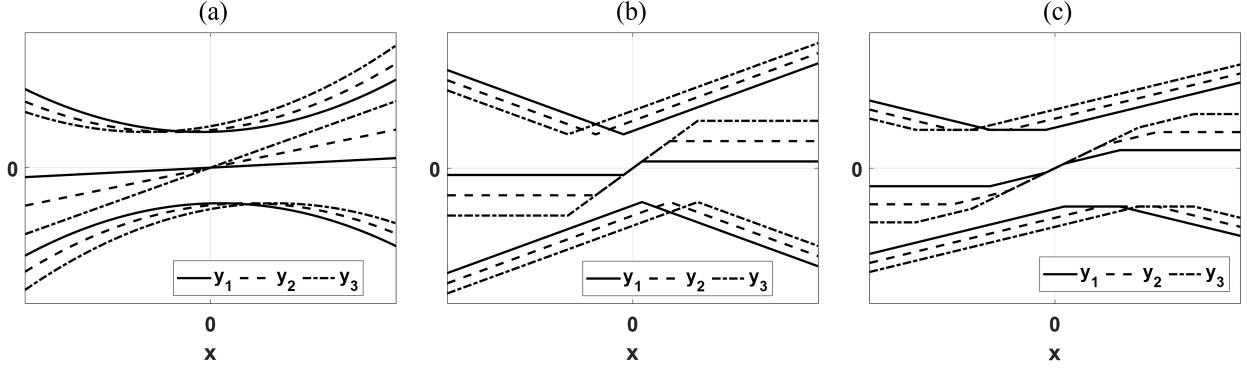


Figure 2: A conceptual scalar demonstration of a) empirical correlators, b) L_1 type correlators, and c) an example of correlators using mixtures of piece-wise linear functions with $L = 1$, $w_1 = 1$, and $\alpha_l = 0.5$. All correlators $f(x, y)$ can be viewed as a difference between $h(x + y)$ and $h(x - y)$. The upper three curves represent $h(x + y)$, the lower three curves represent $-h(x + y)$, and curves in the middle are $f(x, y)$ for different values of $y = y_1, y_2, y_3$.

for the empirical cross-correlator defined in equation 2 which can be expressed as

$$\frac{1}{N} \sum_{n=1}^N x_n y_n = \frac{1}{4N} \sum_{n=1}^N (x_n + y_n)^2 - (x_n - y_n)^2 \quad (7)$$

The symmetric quadratic functions $(x + y)^2$ and $-(x - y)^2$ are shown in Fig. 2(a) which when summed together results in the product xy . When extended to N dimensions, the quadratic functions in equation 2 become L_2 distances $\|\mathbf{x} + \mathbf{y}\|_2^2$ and $-\|\mathbf{x} - \mathbf{y}\|_2^2$ and their sum is proportional to the empirical cross-correlation $\frac{1}{N} \sum_{n=1}^N x_n y_n$. The concept can be generalized to other norms and in Fig. 2(b) we show the equivalent construction for an L_1 type cross-correlators using L_1 distances $|x + y|$ and $-|x - y|$. Both these constructions can be viewed as special cases of mixtures of piece-wise linear functions as shown in Fig. 2(c) and can be expressed as

$$f(x, y) = h(x + y) - h(x - y) \quad (8)$$

where

$$h(x) = \frac{1}{2} \sum_{l=1}^L w_l (|x - \alpha_l| + |x + \alpha_l|), \quad (9)$$

with parameters $\alpha_l \geq 0$, $w_l \geq 0$; $\sum_l w_l = 1$ and $|\cdot|$ is an absolute-value function defined as

$$|x| = \begin{cases} x & ; x \geq 0 \\ -x & ; x < 0 \end{cases} \quad (10)$$

We now state the Lemma that can be used to compute the function $g(R) = \mathcal{E}[f(x, y)]$.

Lemma 2.1. *If the function $f(x, y)$ is given by equation 8 and 9 and if the joint probability distribution of $x \in \mathbb{R}$ and $y \in \mathbb{R}$ are is then given by*

$$p(x, y) = \frac{1}{2\pi\sqrt{1-R^2}} \exp\left[-\frac{x^2 + y^2 - 2Rxy}{2(1-R^2)}\right], \quad (11)$$

where $R \in [-1, 1]$ is the cross-correlation between x and y , then

$$g(R) = \frac{1}{2\sqrt{\pi}} \sum_{l=1}^L \int_0^R \left(\frac{w_l}{\sqrt{(1+\rho)}} \exp\left[-\frac{\alpha_l^2}{4(1+\rho)}\right] + \frac{w_l}{\sqrt{(1-\rho)}} \exp\left[-\frac{\alpha_l^2}{4(1-\rho)}\right] \right) d\rho \quad (12)$$

Proof. Since f is a memory-less function with a well-defined Fourier transform and x and y are zero-mean, unit variance, jointly distributed Gaussian random variables, we can apply Price's theorem [12, 13, 14] which states that

$$\frac{\partial \mathcal{E}(f)}{\partial R} = \mathcal{E} \left[\frac{\partial^2 f}{\partial x \partial y} \right] \quad (13)$$

where the expectation operator \mathcal{E} is defined as

$$\mathcal{E}(f) = \int_{-\infty}^{\infty} \int_{-\infty}^{\infty} f(x, y) p(x, y; \rho) dx dy = g(R). \quad (14)$$

The partial derivatives of the sub-functions $h(x + y)$, $h(x - y)$ in Eqn.9 are

$$\frac{\partial^2 h(x + y)}{\partial x \partial y} = \frac{1}{2} \sum_{l=1}^L w_l [\delta(x + y - \alpha_l) + \delta(x + y + \alpha_l)], \quad (15a)$$

$$-\frac{\partial^2 h(x - y)}{\partial x \partial y} = \frac{1}{2} \sum_{l=1}^L w_l [\delta(x - y - \alpha_l) + \delta(x - y + \alpha_l)]. \quad (15b)$$

where $\delta(\cdot)$ denotes the Dirac-delta function. Substituting in equation 13 leads to

$$\mathcal{E} \left[\frac{\partial^2 h(x + y)}{\partial x \partial y} \right] = \frac{1}{2} \sum_{l=1}^L w_l \int_{-\infty}^{\infty} p(x, -x + \alpha_l) + p(x, -x - \alpha_l) dx, \quad (16a)$$

$$= \frac{1}{\sqrt{\pi(1+R)}} \sum_{l=1}^L w_l \exp \left[-\frac{\alpha_l^2}{4(1+R)} \right], \quad (16b)$$

$$-\mathcal{E} \left[\frac{\partial^2 h(x - y)}{\partial x \partial y} \right] = \frac{1}{2} \sum_{l=1}^L w_l \int_{-\infty}^{\infty} p(x, x - \alpha_l) + p(x, x + \alpha_l) dx, \quad (16c)$$

$$= \frac{1}{\sqrt{\pi(1-R)}} \sum_{l=1}^L w_l \exp \left[-\frac{\alpha_l^2}{4(1-R)} \right]. \quad (16d)$$

Thus, using $f = h(x + y) - h(x - y)$ and from 13

$$\frac{\partial g}{\partial R} = \frac{1}{\sqrt{\pi(1+R)}} \sum_{l=1}^L w_l \exp \left[-\frac{\alpha_l^2}{4(1+R)} \right] + \frac{1}{\sqrt{\pi(1-R)}} \sum_{l=1}^L w_l \exp \left[-\frac{\alpha_l^2}{4(1-R)} \right] \quad (17)$$

leads to the expression for $g(R)$,

$$g(R) = \int_0^R \frac{1}{\sqrt{\pi(1+\rho)}} \sum_{l=1}^L w_l \exp \left[-\frac{\alpha_l^2}{4(1+\rho)} \right] + \frac{1}{\sqrt{\pi(1-\rho)}} \sum_{l=1}^L w_l \exp \left[-\frac{\alpha_l^2}{4(1-\rho)} \right] d\rho \quad (18)$$

□

Even though the equation 12 may not be solved in closed-form, it is analytical and hence can be used to visualize the form of $g(R)$ for specific choices of α_l and w_l . The partial derivative equation in 17 is also useful for choosing appropriate offsets to construct desired correlators, and the derivative when there is only one offset is visualized in Fig. 3 for different values of the offset.

Example 1: When $L = 1$, $w_1 = 1$, $\alpha_1 = 0$, the function f is reduced to

$$f(x, y) = |x + y| - |x - y|, \quad (19)$$

which is the well-studied linear rectifier correlator [13]. In this case, the relation 12 can be evaluated in closed form and is given by

$$g_{L1}(R) = \frac{2}{\sqrt{\pi}} (\sqrt{1+R} - \sqrt{1-R}). \quad (20)$$

Example 2: When $w_l = 1/L$, $\alpha_l = c/L$, $l = 1, \dots, L$ and $c, L \rightarrow \infty$, the function f is reduced to

$$f(x, y) = \frac{1}{2c} ((x + y)^2 - (x - y)^2), \quad (21)$$

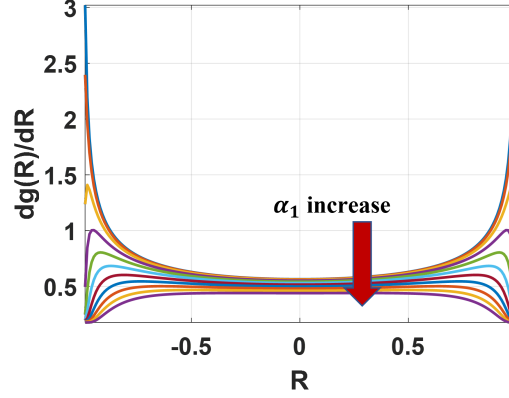


Figure 3: $\frac{\partial g}{\partial R}$ for $L = 1, w_1 = 1$, and $\alpha_1 = \{0, 0.1, 0.2 \dots 1\}$.

where $c > |x|$ is the range of inputs. So the function f becomes the empirical correlator. In this case, the summation in the relation 12 can be replaced by integrals in the limit $L \rightarrow \infty$ in which case

$$\begin{aligned} \frac{\partial g_{L2}}{\partial R} &= \frac{1}{c\sqrt{\pi(1+R)}} \int_0^\infty \exp\left[-\frac{x^2}{4(1+R)}\right] dx \\ &\quad + \frac{1}{c\sqrt{\pi(1-R)}} \int_0^\infty \exp\left[-\frac{x^2}{4(1-R)}\right] dx \\ &= \frac{2}{c}. \end{aligned} \quad (22)$$

Therefore, $g_{L2}(R) = \frac{2}{c}R$ matches the result for a scaled empirical cross-correlation. The $g(R)$ of both empirical and linear rectifier correlators are shown in Fig. 4(a).

Let's denote $\mathcal{E}(f)$ or $g(R)$ by y , we can derive the following from $g_{L1}(R)$ in 20

$$R^2 = \frac{\pi}{4}y^2 - \frac{\pi^2}{64}y^4. \quad (23)$$

This suggests that g^{-1} in Fig. 1 can be robustly estimated using a polynomial expansion with a relatively low degree. This is important since the closed-form solution for equation 18 can not be computed for different choices of w_l, α_l . As a result, g^{-1} has to be learned/estimated by drawing samples with known apriori cross-correlation, which is then used to estimate R according to Fig. 1. As we will show later in section 3, this calibration procedure and procedure to estimate R can be agnostic to the input distribution.

We now apply the calibration procedure to three other types of functions of the type given by expression 8. The first is a margin-propagation (MP) function that can be constructed using a finite number of splines L and self-normalizes itself such that the maximum gradient $|f'| \leq 1$. The MP function is given by

$$(x - z)_+ + (-x - z)_+ = \gamma, \quad (24)$$

$$h(x) = z, \quad (25)$$

where $(\cdot)_+$ is a rectifying linear unit (ReLU) function, and $\gamma > 0$ is a hyper-parameter.

The second function is the Huber function [15] which requires an infinite number of splines and is given by

$$h(x) = \begin{cases} 0.5x^2/\sigma, & x < \sigma \\ |x| - \frac{1}{2}\sigma, & x \geq \sigma, \end{cases} \quad (26)$$

where $\sigma > 0$ is a threshold parameter. Note that the maximum gradient of the Huber function is 1.

The third function is a log-sum-exp (LSE) function which also requires an infinite number of splines and is given by

$$h(x) = \frac{1}{a}(\log(\exp[ax] + \exp[-ax])), \quad (27)$$

where $a > 0$ is a scaling factor. Note that the maximum gradient of the log-sum-exp function is also 1.

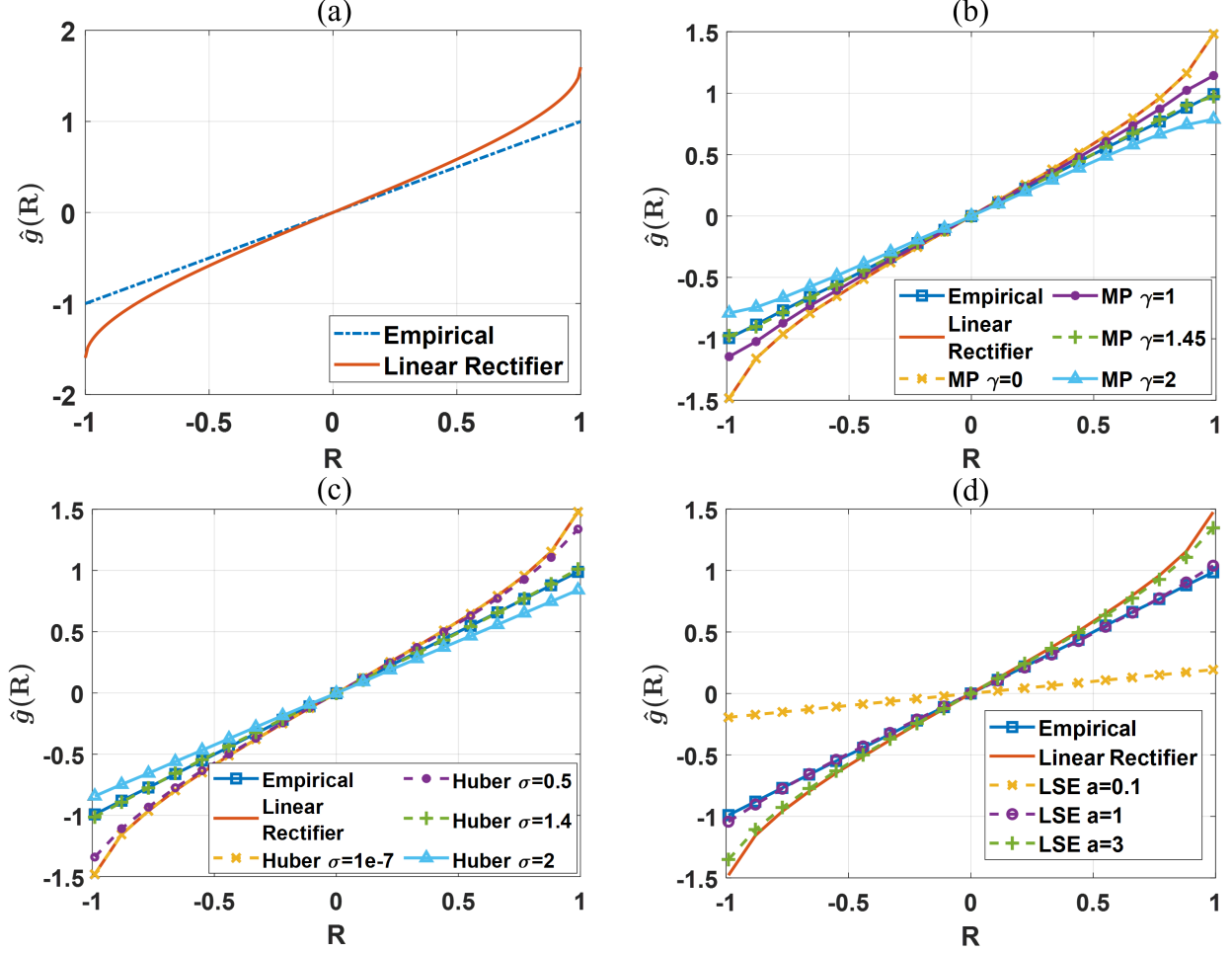


Figure 4: The normalized $g_{L1}(R)$ and $g_{L2}(R)$ and the estimated $\hat{g}(R)$ for the MP, Huber, and LSE functions for standard bivariate normal distributions from Monte Carlo experiments. The expected output of the empirical and linear rectifier correlators are added for comparison. a) The normalized $g_{L1}(R)$ and $g_{L2}(R)$; b) The $\hat{g}(R)$ of MP correlators with $\gamma = \{0, 1, 1.45, 2\}$; c) The $\hat{g}(R)$ of Huber correlators with $\sigma = \{10^{-7}, 0.5, 1.4, 2\}$; d) The $\hat{g}(R)$ of LSE correlators with $a = \{0.1, 1, 3\}$.

Fig. 4b),c), and d) shows the average output of cross-correlation function $\hat{g}(R)$ corresponding to the MP, Huber and LSE functions, which is used as an approximation of the correlation function $g(R)$ to get the calibration function g^{-1} . It can be observed from Fig. 4c) and d) that the $g(R)$ for the Huber and LSE functions are bounded above by $g_{L1}(R)$ and the magnitude of gradient $|\frac{\partial g}{\partial R}|$ monotonically increases as R increases. In fact, the normalized $g(R)$ for the Huber function and LSE functions are bounded above and below by the normalized $g_{L1}(R)$ and $g_{L2}(R)$. For Huber functions, it's a combination of the quadratic function (L_2) and absolute value function (L_1). As the threshold value σ increases, its output is closer to the empirical correlator. Conversely, it becomes a linear rectified correlator when σ is sufficiently small. For LSE functions, as the scaling factor a increases, the $h(x)$ for LSE functions in expression 27 can be simplified to $\frac{1}{a} \log(\exp[a|x|]) = |x|$ as the negative part will go to zero exponentially fast. On the other hand, as a decreases, the function $h(x)$ can be approximated by the Taylor series expanded at zero, which leads to the following

$$h(x) = \frac{1}{a} \log\left(\sum_{n=0}^{\infty} \frac{(ax)^n}{n!} + \frac{(-ax)^n}{n!}\right). \quad (28)$$

The odd-degree terms cancel each other out and higher-order terms decay fast, which leads to

$$h(x) \approx \frac{1}{a} \log(2 + (ax)^2). \quad (29)$$

Applying the same trick to the logarithm but expanding at 2, we have

$$h(x) \approx \frac{1}{a}(\log(2) + \frac{1}{2}(ax)^2 + \dots) \approx \frac{1}{a} + \frac{1}{2}ax^2. \quad (30)$$

Therefore, the LSE correlator approaches the empirical correlator as a decreases. Since the normalized $g(R)$ of Huber and log-sum-exp correlators fall between $g_{L1}(R)$ and $g_{L2}(R)$ and the magnitude of gradient $|\frac{\partial g}{\partial R}|$ monotonically increases as R increases, the inverse cross-correlation function g^{-1} can be approximated by a polynomial of degree lower or equal to the degree needed for g_{L1}^{-1} . In practice, we found that fourth order polynomial is sufficient for calibration of g_{L1}^{-1} . For calibrating MP correlators, higher degree polynomials were needed as the value of γ increases as its $|\frac{\partial g}{\partial R}|$ is not monotonically increasing as correlation increases. As such, a fifth-order polynomial was used to learn the inverse cross-correlation function g^{-1} .

3 Extension to non-Gaussian distributions

The theoretical and experimental results presented in section 2 assumed random variables with joint Gaussian distributions. In this section, we extend the previous results for non-Gaussian distributions. To achieve this, we use results from the Hyperdimensional computing literature, which state that variances and cross-correlations are preserved when random variables are mapped into high-dimensional space using Unitary random matrices.

Lemma 3.1. *Let x and y be zero-mean random variables with unit variance and with a cross-correlation R . Let $\Phi : \mathbb{R}^N \rightarrow \mathbb{R}^M$ denote a high-dimensional embedding using a Unitary transform such that $\mathcal{E}[\Phi(\mathbf{x})] = \mathbf{0}$. Then, as $N \rightarrow \infty$, $\frac{1}{N} \langle \Phi(\mathbf{x}), \Phi(\mathbf{y}) \rangle \rightarrow R$, where $\langle \cdot, \cdot \rangle$ is the inner product.*

Proof. Suppose \mathbf{x} and \mathbf{y} are \mathbb{R}^N -valued random vector, and each entry x_n, y_n are independently identically distributed (i.i.d) variables with the joint probability density function $p(x, y; R)$

$$\frac{1}{N} \langle \Phi(\mathbf{x}), \Phi(\mathbf{y}) \rangle = \frac{1}{N} \langle \mathbf{x}, \mathbf{y} \rangle = \frac{1}{N} \sum_{n=1}^N x_n y_n \xrightarrow{N \rightarrow \infty} R \quad (31)$$

□

The Walsh-Hadamard-Transform is one such unitary transform $\mathcal{H} : \mathbb{R}^N \rightarrow \mathbb{R}^N$ and it can be represented by a $N \times N$ Hadamard matrix. An example 4×4 WHT matrix is shown below

$$H_4 = \frac{1}{2} \begin{pmatrix} 1 & 1 & 1 & 1 \\ 1 & -1 & 1 & -1 \\ 1 & 1 & -1 & -1 \\ 1 & -1 & -1 & 1 \end{pmatrix} \quad (32)$$

The Hadamard matrices are orthogonal and symmetric matrices composed of +1 and -1 with a normalization factor $1/\sqrt{N}$, which makes it easy for implementations and computations. Besides keeping the covariance between random variables, it can also be shown that the transformed zero-mean variables converge to the joint Gaussian distribution with the same variance and covariance.

Lemma 3.2. *Let X and Y be zero-mean random variables with unit variance and with a cross-correlation R . Let $\mathcal{H} : \mathbb{R}^N \rightarrow \mathbb{R}^N$ denote the Walsh-Hadamard-Transform. Suppose the entries of the vector equation $x' = \mathcal{H}(x)$ are given by $x'_n = h_n(x_1, \dots, x_n)$, and $h_n(\cdot)$ is therefore*

$$h_n(x_1, \dots, x_n) = \begin{cases} \frac{1}{\sqrt{N}} \sum_{n=1}^N x_n, & n = 1, \\ \frac{1}{\sqrt{N}} (\sum_{n=1}^{N/2} x_n - \sum_{n=1}^{N/2} x_n), & n \neq 1, \end{cases} \quad (33)$$

where the x_n are independently identically distributed (i.i.d.) samples from X . Then, as $N \rightarrow \infty$, the joint probability distribution $p(x'_n, y'_n)$ converges to a bivariate Gaussian distribution with zero-mean, unit variance and covariance R .

Proof. Suppose X and Y are zero-mean random variables with finite variances and covariance R . According to the multivariate Central Limit Theorem (CLT) [16], as $N \rightarrow \infty$ the joint distribution $p(\sqrt{N}\bar{X}_N, \sqrt{N}\bar{Y}_N)$ converges to bivariate Gaussian distribution with zero mean and the same variances and covariance R , where $\bar{X} = \frac{1}{N} \sum_{n=1}^N x_n$ is the average of N independently identically distributed samples of X .

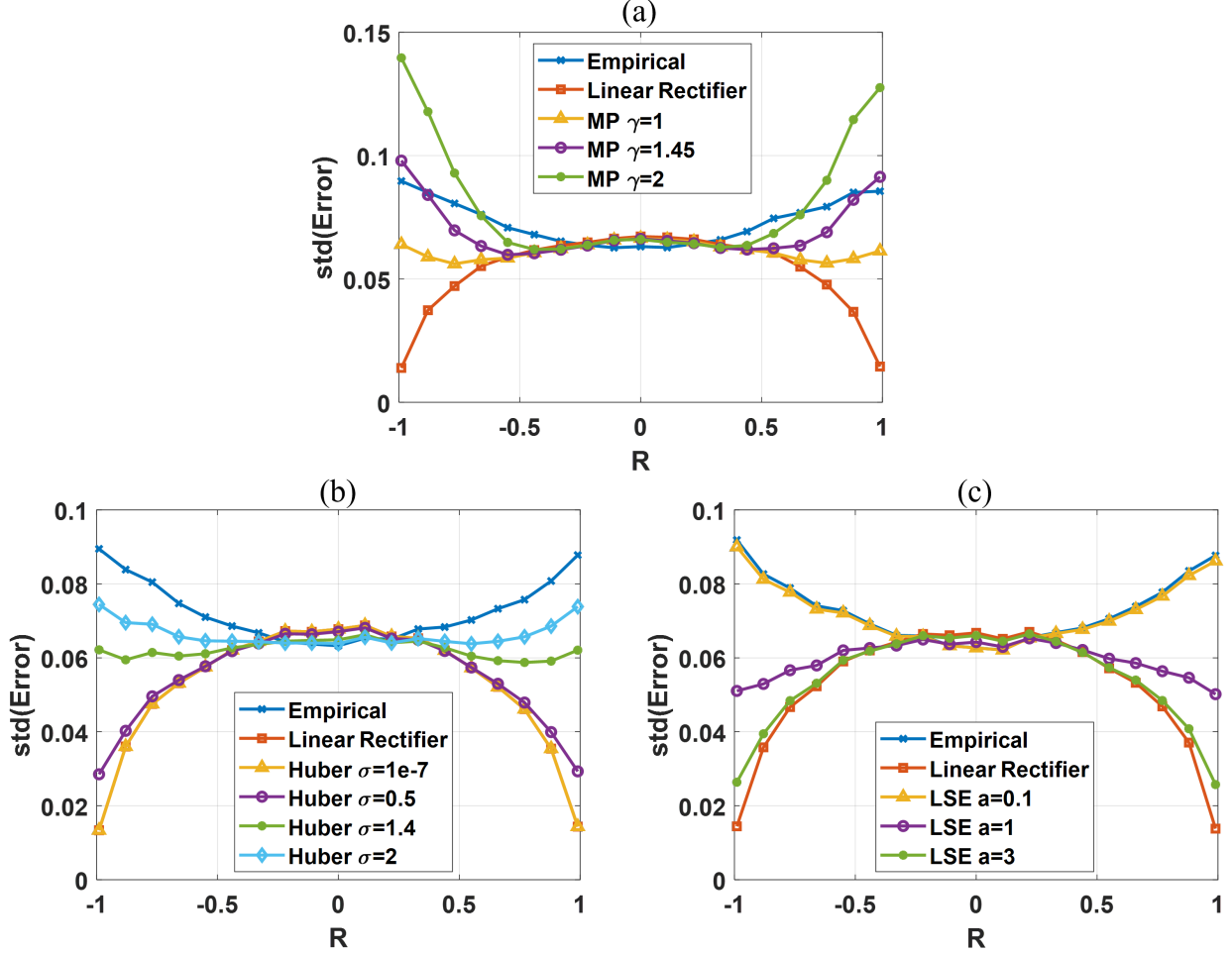


Figure 5: The standard deviation of cross-correlation estimation error of MP, Huber, and LSE correlators for different correlation levels at the dimension of 256, with the SNR of empirical and linear rectifier added for reference. a) The error plot of MP correlators with $\gamma = \{1, 1.45, 2\}$; b) The error plot of Huber correlators with $\sigma = \{10^{-7}, 0.5, 1.4, 2\}$; c) The error plot of LSE correlators with $a = \{0.1, 1, 3\}$.

Notice that the transformed entry after WHT $x'_n = h_n(x_1, \dots, x_n)$ can be expressed as

$$x'_n = \begin{cases} \sqrt{N}\bar{X}_N, & n = 1, \\ \frac{1}{\sqrt{2}}\sqrt{\frac{N}{2}}(\bar{X}_{N/2} - \bar{X}_{N/2}), & n \neq 1. \end{cases} \quad (34)$$

For $n = 1$, the CLT obviously applies to the transformed input x'_1 and y'_1 . For the case of $n \neq 1$, note that the CLT also applies to $\pm\sqrt{\frac{N}{2}}\bar{X}_{N/2}$ and $\pm\sqrt{\frac{N}{2}}\bar{Y}_{N/2}$, so they become bivariate Gaussian with zero mean, and same variances and covariance, and so is their sum divided by $\sqrt{2}$. \square

As such, using the proof in section 2, it can be shown that for correlators that can be expressed by equations 8 and 9, the expected output $\mathcal{E}[f(\mathcal{H}(x), \mathcal{H}(y))]$ is equal to $g(R)$. In other words, for non-Gaussian distributed variables with zeros mean and finite covariance R , we can first transform the inputs to jointly Gaussian distribution, which preserves the covariance R , and then use the cross-correlator in section 2 to estimate the cross-correlation R using the transformed data and the same g^{-1} .

4 Experiments Results and Analysis

4.1 Experiments and Results for Jointly Gaussian Inputs

This section presents the results using different correlators to estimate the covariance for standard jointly normal distribution. To study and compare their performance, vectors of different lengths are randomly sampled from the zero mean and unit variance Gaussian distribution. Each vector pair $S_1, S_2 \in \mathbb{R}^D$ is mixed in the following way to generate a bivariate Gaussian distribution $X = (X_1, X_2)$ with different correlation R to learn and test the inverse cross-correlation function $g(R)$,

$$X_1 = S_1, \quad (35)$$

$$X_2 = RS_1 + \sqrt{1 - R^2}S_2, \quad (36)$$

$$X = (X_1, X_2) \sim N(\vec{0}, \Sigma), \Sigma = \begin{pmatrix} 1 & R \\ R & 1 \end{pmatrix}. \quad (37)$$

In Fig. 5 we display the standard deviation of cross-correlation estimation errors made by the MP, Huber, and LSE

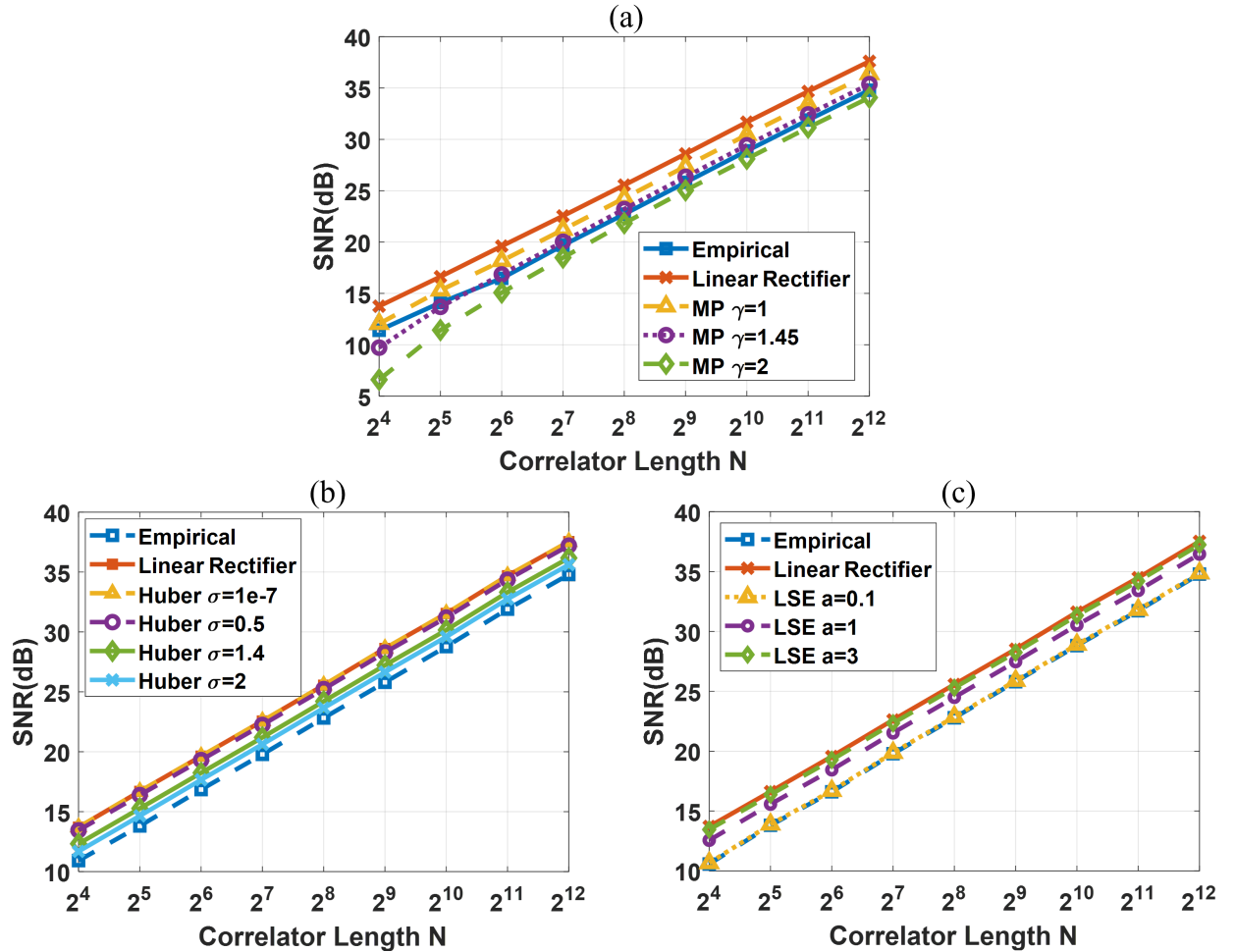


Figure 6: The SNR plots of MP, Huber, and LSE correlators from correlator length of 16 to 65536, with the SNR of empirical and linear rectifier correlators as a reference. a) The SNR plot of MP correlators with $\gamma = \{1, 1.45, 2\}$; b) The SNR plot of Huber correlators with $\sigma = \{10^{-7}, 0.5, 1.4, 2\}$; c) The SNR plot of LSE correlators with $a = \{0.1, 1, 3\}$.

correlators with different parameters at different levels of cross-correlation using the learned inverse cross-correlation function g^{-1} . It is observed that the linear rectifier correlator is more accurate when the signal of interest is highly correlated, while the empirical correlator makes less error in the other case. As discussed in section 2, the Huber, and LSE correlators behave more like the empirical correlator when σ is high and a is small, and approach the linear

rectifier correlator otherwise. The MP correlators using the function 24 is equivalent to the linear rectifier correlator when $\gamma = 0$. As γ increases, the performance degrades and performs even worse than the empirical correlator.

In Fig. 6, we plot the signal-to-noise-ratio (SNR) for each of these five cross-correlators for different sample sizes or correlation-window sizes N . The result shows that for joint Gaussian input distribution, the linear rectifier-based correlator shows the best SNR. Also, the SNR increases by 3dB when the correlation length N is doubled. This result can be attributed to the reduction in the estimation error due to simple averaging.

4.2 Non-Gaussian Inputs and Walsh-Hadamard-Transformation

In this section, the WHT method was tested on non-Gaussian distributions to verify that the function $g(R)$ remains unchanged for non-Gaussian inputs after being transformed by the WHT. Fig. 7 presents the distribution of random vectors used in the experiment. The first non-Gaussian distribution tested shown in Fig. 7(a) has zero mean, unit variance uniform marginal distributions. In this case, the original joint distribution is symmetric. The second non-Gaussian distribution tested shown in Fig. 7(b) has asymmetric zero mean unit variance marginal input distributions. In particular, the marginal distribution of the Y vector is composed of samples drawn from two normal distributions with opposite mean and unequal variance with equal possibilities. From Fig. 7, it can be seen that the vectors are jointly Gaussian distributed after the transformation. Monte Carlo experiments show that the expected correlator output $\mathcal{E}[f(\mathcal{H}(x), \mathcal{H}(y))]$ is the same as the $g(R)$ for jointly Gaussian inputs. So no calibration is needed to learn g^{-1} for different distributions.

On the other hand, it should be noticed that the standard deviation of cross-correlation estimation errors is not guaranteed to be the same for different distributions, even after the WHT transformation. To see this, notice that the WHT process will not change the output for the empirical correlator, because the WHT transformation is unitary. However, the estimation errors made by the empirical correlator, which is equivalent to

$$Var(XY - \mathcal{E}[XY]) = \mathcal{E}[(XY)^2] - g(R)^2 = \int_{-\infty}^{\infty} \int_{-\infty}^{\infty} X^2 Y^2 p(x, y) dx dy - g(R)^2, \quad (38)$$

will change as the joint probability density function $p(x, y)$ changes for varying distributions. In particular, for jointly Gaussian distribution, it can be verified that $Var(XY - \mathcal{E}[XY]) = 1 + R^2$, whereas it is $1 - \frac{1}{5}R^2$ in the case of jointly uniform distribution in the symmetric experiment. The standard deviation of estimation error plots for the symmetric non-Gaussian test and the asymmetric test are displayed in Fig. 8 and 9. It is observed that the contour of the error plot changes for all correlators except the linear rectifier correlator, which is still the best-performing cross-correlation estimator in these two specific non-Gaussian input distributions.

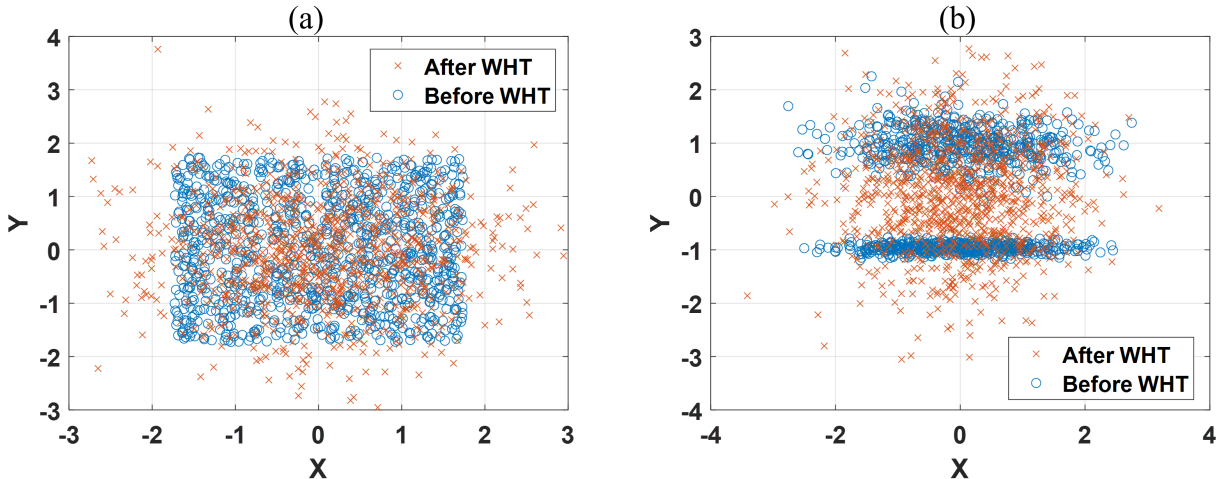


Figure 7: The distribution of the random vectors with zero correlation before and after the WHT transformation. a) The random vectors for the symmetric non-Gaussian distribution test. Original X and Y are uniformly distributed with zero mean and unit variance; b) The asymmetric non-Gaussian distribution, where the marginal distribution for X follows the standard normal distribution before WHT, and Y is a mixture of two normal distributions with opposite mean and unequal variance. Y is zero mean and unit variance as well.

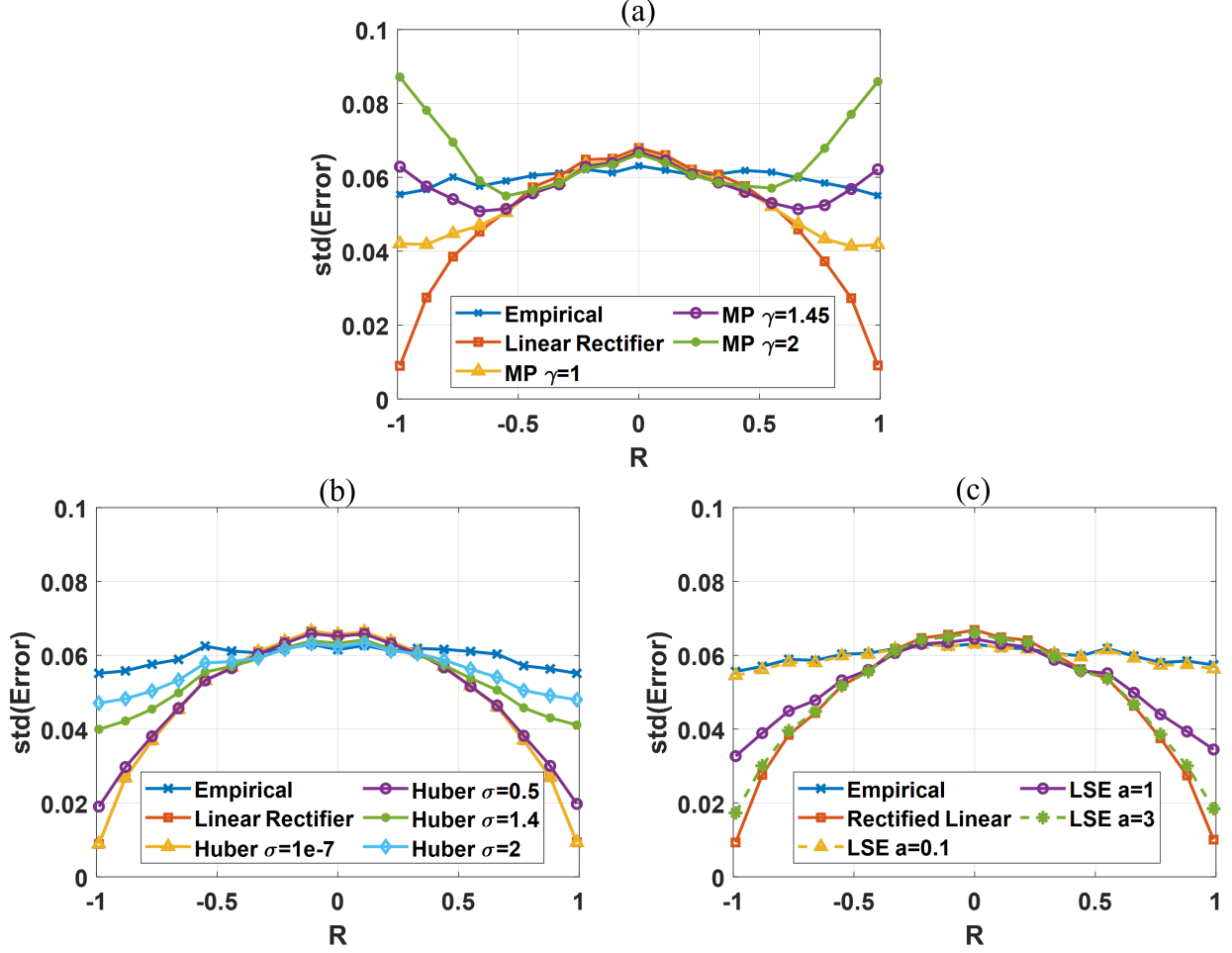


Figure 8: The standard deviation error plot of MP, Huber, and LSE correlators for the symmetric input distribution test when dimension is 256. a) The error plot of MP correlators with $\gamma = \{1, 1.45, 2\}$; b) The error plot of Huber correlators with $\sigma = \{10^{-7}, 0.5, 1.4, 2\}$; c) The error plot of LSE correlators with $a = \{0.1, 1, 3\}$.

5 Discussions and Conclusions

In this paper, we presented a mathematical framework for analyzing different types of online cross-correlators. The analysis has been verified by Monte-carlo simulation for different input distributions. However, error analysis reveals that the shape of the error profile exhibits a trade-off. Online cross-correlation estimators that exhibit high errors near $R \approx 0$ make fewer errors near $|R| \approx 1$. The hyperparameters of the Huber estimators, MP estimators, and log-sum-exp estimators can be adapted to achieve different error profiles.

However, the complexity of implementing these different online estimators on hardware could be significantly different. The Huber cross-correlator relies on the quadratic function and hence may be difficult to implement on hardware. On the other hand, the MP and LSE correlators can be easily implemented on analog hardware [17]. Even though MP and LSE cross-correlators require calibration to estimate the function g^{-1} , we show that the calibration process can be agnostic to input distributions using the WHT transformation.

Another potential brought by other correlators is the advantage of computational complexity and dynamic range when implementing on digital systems. It is obvious that the computation of the linear rectifier correlator and the MP correlator (without additional offsets) is much cheaper than the empirical correlator as it uses only additions [18]. The addition operation is immune to underflow on a fixed point system. The LSE correlator also possesses the advantage of numerical stability at the cost of computational complexity. It is a common trick used in machine learning to address the issue of gradient updates.

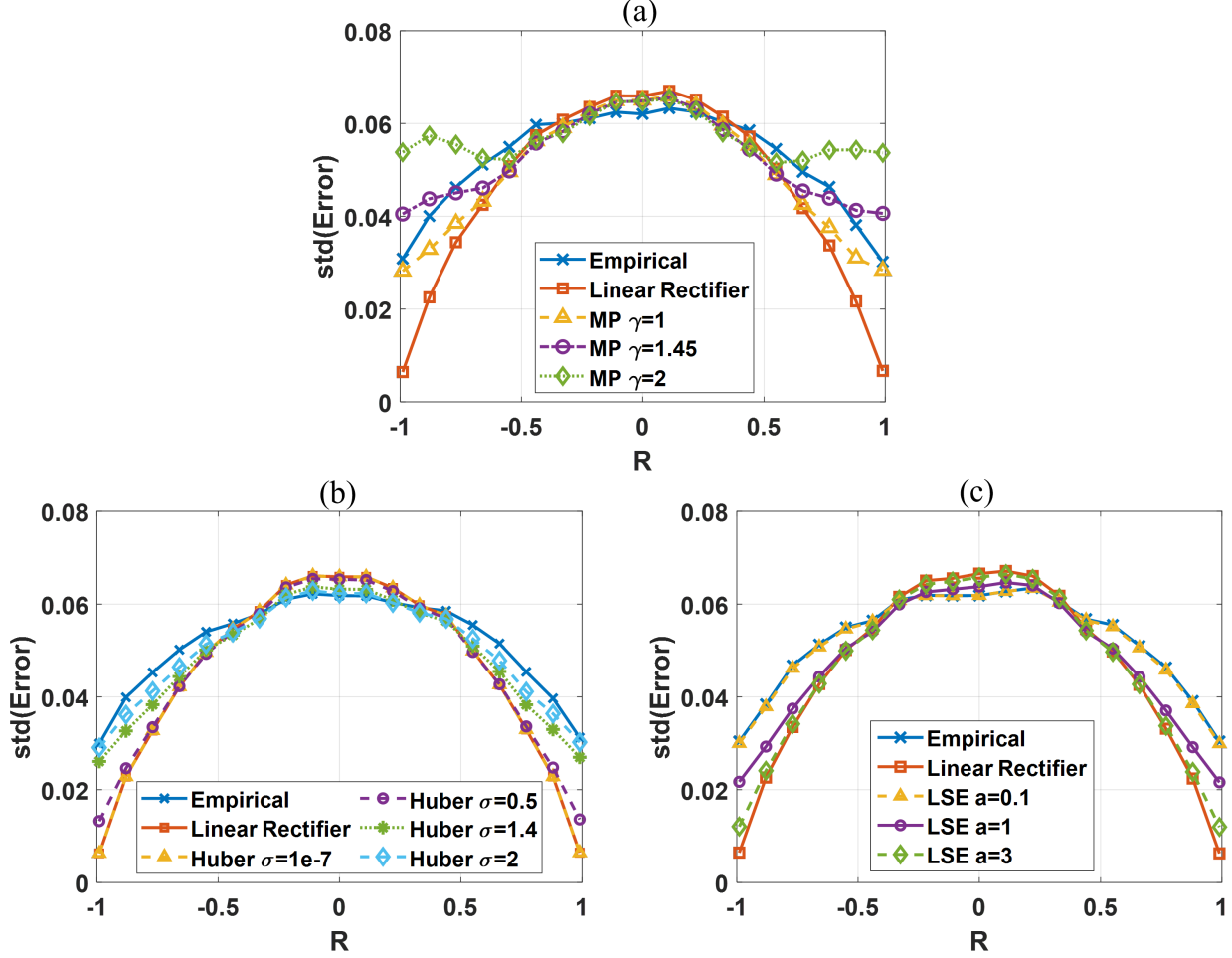


Figure 9: The standard deviation of cross-correlation estimation error of MP, Huber, and LSE correlators for the asymmetric input distribution at dimension of 256. a) The error plot of MP correlators with $\gamma = \{1, 1.45, 2\}$; b) The error plot of Huber correlators with $\sigma = \{10^{-7}, 0.5, 1.4, 2\}$; c) The error plot of LSE correlators with $a = \{0.1, 1, 3\}$.

In terms of accuracy for estimating the cross-correlation of jointly Gaussian distributed inputs, we can see that the empirical method may not be the best correlator. The linear rectifier correlator is the best in estimating the covariance for highly correlated signals and in terms of overall SNR. The Huber and LSE correlator’s performance is bounded by the linear rectifier and empirical correlator. The MP correlators using the function 24 is equivalent to the linear rectifier correlator when $\gamma = 0$. As γ increases, its performance for higher γ values can be potentially improved by introducing offsets. Of course, the above observations are not guaranteed to hold for other input distributions and are left for future research.

References

- [1] D.S. Moore, G.P. McCabe, and B.A. Craig. *Introduction to the Practice of Statistics*. W. H. Freeman, 2014.
- [2] Y. Lecun, L. Bottou, Y. Bengio, and P. Haffner. Gradient-based learning applied to document recognition. *Proceedings of the IEEE*, 86(11):2278–2324, 1998.
- [3] K.I. Diamantaras and Sun-Yuan Kung. Cross-correlation neural network models. *IEEE Transactions on Signal Processing*, 42(11):3218–3223, 1994.
- [4] Jae-Chern Yoo and Tae Hee Han. Fast normalized cross-correlation. *Circuits, systems and signal processing*, 28:819–843, 2009.

- [5] S. Adrián-Martínez, M. Ardid, M. Bou-Cabo, I. Felis, C. Llorens, J. A. Martínez-Mora, and M. Saldaña. Acoustic signal detection through the cross-correlation method in experiments with different signal to noise ratio and reverberation conditions, 2015.
- [6] Gilbert Strang. *Linear algebra and its applications*. Thomson, Brooks/Cole, Belmont, CA, 2006.
- [7] Tomas Mikolov, Ilya Sutskever, Kai Chen, Greg S Corrado, and Jeff Dean. Distributed representations of words and phrases and their compositionality. In C.J. Burges, L. Bottou, M. Welling, Z. Ghahramani, and K.Q. Weinberger, editors, *Advances in Neural Information Processing Systems*, volume 26. Curran Associates, Inc., 2013.
- [8] Chen Wang, Wenshan Wang, Yuheng Qiu, Yafei Hu, and Sebastian A. Scherer. Visual memorability for robotic interestingness via unsupervised online learning. *CoRR*, abs/2005.08829, 2020.
- [9] Chen Wang, Le Zhang, Lihua Xie, and Junsong Yuan. Kernel cross-correlator. *Proceedings of the AAAI Conference on Artificial Intelligence*, 32, 2018.
- [10] Pentti Kanerva. Hyperdimensional computing: An introduction to computing in distributed representation with high-dimensional random vectors. *Cognitive Computation*, 1:139–159, 2009.
- [11] Anthony Thomas, Sanjoy Dasgupta, and Tajana Rosing. A theoretical perspective on hyperdimensional computing. *J. Artif. Int. Res.*, 72:215–249, jan 2022.
- [12] R. Price. A useful theorem for nonlinear devices having gaussian inputs. *IRE Transactions on Information Theory*, 4(2):69–72, 1958.
- [13] E. McMahon. An extension of price’s theorem (corresp.). *IEEE Transactions on Information Theory*, 10(2):168–168, 1964.
- [14] A. Papoulis. Comments on ‘an extension of price’s theorem’ by mcmahon, e. l. *IEEE Transactions on Information Theory*, 11(1):154–154, 1965.
- [15] Peter J. Huber. Robust Estimation of a Location Parameter. *The Annals of Mathematical Statistics*, 35(1):73 – 101, 1964.
- [16] Achim Klenke. *Probability Theory: A Comprehensive Course*. Springer, 2007.
- [17] Ming Gu and Shantanu Chakrabartty. Synthesis of bias-scalable cmos analog computational circuits using margin propagation. *IEEE Transactions on Circuits and Systems I: Regular Papers*, 59(2):243–254, 2012.
- [18] Abhishek Ramdas Nair, Pallab Kumar Nath, Shantanu Chakrabartty, and Chetan Singh Thakur. Multiplierless mp-kernel machine for energy-efficient edge devices. *IEEE Transactions on Very Large Scale Integration (VLSI) Systems*, 30(11):1601–1614, 2022.